Morphology and Properties of Poly(vinyl Chloride)–Polyurethane Blends

CARL B. WANG and STUART L. COOPER, *Department of Chemical Engineering, University of Wisconsin, Madison, Wisconsin 53706*

Synopsis

The objective of this research was to study the morphology and properties of PVC–polyurethane blends. Studies on blends of a segmented polyether polyurethane with PVC were carried out utilizing differential scanning calorimetry, Rheovibron, stress–strain, infrared peak position studies, and infrared dichroism experiments. This thermodynamically incompatible system was made kinetically compatible by precipitation from tetrahydrofuran (THF) solutions. THF–dioxane solution casting and melt processing produced an incompatible system. The compatible polyurethane–PVC system contains a well-mixed PVC–polyether matrix phase as evidenced by T_g shifts, orientation characteristics, and infrared peak position changes. The aromatic urethane segments which exhibit microphase separation in the pure polyurethane are not solubilized by blending with PVC by any of sample preparation methods used in this study.

INTRODUCTION

Compatible polyblend systems are usually denoted as having a single glass transition temperature somewhere between those of the pure blend components. Such blends will have a narrow glass transition range in temperature or frequency and will have a T_g which is predictable using the various equations applied to random copolymers. Various methods have been used to determine the compatibility of polyblends, with each one having its advantages and sensitivity. Thus, microscopic methods using transmission electron microscopy (TEM),[1,2] scanning electron microscopy (SEM),[1,3,4] glass transition temperature studies using thermal analysis tests,[5] dynamic mechanical and dielectric testing,[6–8] NMR,[9] FTIR,[10] and stress–strain[11] measurements have all been used. Of the methods listed, microscopy, glass transition temperature measurements, and dynamic mechanical testing have been most valuable in studies of the polyblend compatibility. However, it should be noted that a given system which appears compatible by one method may be incompatible by another.[12]

The morphology of polymer blends is intimately correlated with the properties of the system.[13,14] Because polyblend compatibility is a relative term, the domain size is often used to indicate the extent of mixing, i.e., the smaller the domains, the more compatible the system.[15] Other morphological variables include domain topology and the discrimination between the maxtrix and dispersed phase. It is also noted that all properties concerned with transport processes, such as diffusion and permeation,[16] acoustic damping,[17] and electrical or heat conduction, necessarily depend on the phase structure.

It is well known that compatible polyblends are rare.[18,19] However, PVC, by

Journal of Applied Polymer Science, Vol. 26, 2989–3006 (1981)
 CCC 0021-8995/81/092989-18$01.80

virtue of the weakly "acidic" or proton-donating α-hydrogen,

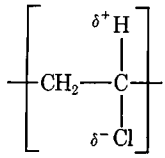

has been shown to exhibit miscibility with a considerable number of polymers. In addition, the practical purpose of studying PVC blends is to develop a permanently plasticized, high impact-strength material via incorporation of a low T_g polymer which is compatible with PVC. The polymers which are compatible with PVC include butadiene–acrylonitrile copolymers,[20] segmented polyether ester copolymers,[5,7,17] and poly-ϵ-caprolactone,[21,22] among others.

The purpose of this study was to discover the effect of sample preparation methods upon the morphology of polyurethane–PVC blends.

EXPERIMENTAL

Materials

The polyether-based polyurethane studied was prepared by the B. F. Goodrich Company and has been designated ET-38-1 in earlier studies.[23,24] The hard segment is composed of 4,4′-diphenylmethane diisocyanate (MDI) chain extended with butane diol (BD), while poly(tetramethylene oxide) (PTMO) is used as the soft segment. The sample code of ET-38-1 represents the type of the soft segment (ET), the weight percent of MDI present (38%), and the approximate soft segment molecular weight in thousands (1). Schematically, the chemical structure of ET-38-1 is

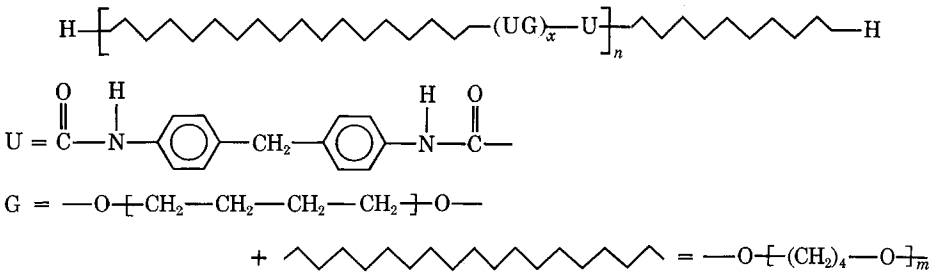

The parameters n, x, and m are approximately 45, 2, and 14. The PVC used was Union Carbide's QYTQ-387 having $\overline{M}_n$ = 35,000 and $\overline{M}_w$ = 72,000.

Sample Preparation

The samples were divided into three series: (1) spin-cast[25] films of a solution of the polymers dissolved in tetrahydrofuran (THF); (2) spin-cast films of a solution of polymers dissolved in a solvent mixture of THF and *p*-dioxane (volume ratio 1:1); and (3) spin-cast films prepared in the same way as series 1, but followed by compression molding. It should be noted that while the polyurethane was soluble in both THF and dioxane, PVC was soluble in THF and THF/dioxane, not dioxane alone. The sample compositions were identified as (the weight percent of ET-38-1)/(the weight percent of PVC); and except for pure ET-38-1, 1 wt % Ferro GH-148 liquid thermostabilizer (Ferro Corporation) was added to each of the polymer solutions, based on the weight of PVC. The spin-cast films were dried in a vacuum oven at 70°C for one week and then stored in a desiccator at room temperature.

It should be mentioned that under these drying conditions, a slight amount of THF may be retained in the PVC cast films which causes a depression of T_g as indicated by the DSC data. The severity of this problem depends on the percent PVC content in the blends and the thickness of the film. Thus, except for pure PVC and the 10/90 blends, the solvent remaining in these systems is small enough to not seriously affect the experimental results. Moreover, the IR specimens should contain a negligible amount of solvent as they are very thin ($\sim 10\mu$ in thickness). Higher drying temperatures which more thoroughly removed the last traces of solvent in the PVC-rich blends tended to degrade the PVC.

Experimental Methods

DSC thermograms over the temperature range −100 to 200°C were recorded using a Perkin–Elmer DSC II at a heating rate of 20°C/min under a He purge. Sample weights were 22 ± 3 mg.

Rheovibron dynamic mechanical data were obtained at 110 Hz using a Rheovibron DDV-II viscoelastometer (Toyo Measuring Instruments). Samples were initially cooled to −150°C, and measurements were made at 3°C intervals with a heating rate of 2.5°C/min.

Uniaxial stress–strain experiments were made using an Instron tensile testing apparatus at room temperature, with a crosshead speed of 0.5 in./min and a gauge length of 1.5 in. Samples were cut with an ASTM 412 die. The percentage elongation was measured using an extensometer accessory.

Survey IR spectra of samples were obtained using a Perkin–Elmer model 180 infrared spectrophotometer. The peak positions for the specific functional groups (e.g., N—H, C=O, and C—Cl) were determined to the nearest 0.1 cm^{-1}.

Infrared dichroism was accomplished using a stretching device which elongated the sample from both ends simultaneously. The jig was mounted in the path of the sample beam at a 45° angle. An internal polarizer was set 45° or −45°, respectively, for recording $A_\parallel$ or $A_\perp$. Ten minutes of stress relaxation was allowed for the samples to approach equilibrium before the $A_\parallel$ and $A_\perp$ spectra were recorded.

Infrared dichroism occurs because absorption by a particular functional group occurs only at a specific angle which is represented by a transition moment vector

M. If a polymer is elongated such that the M vectors are preferentially oriented, the amount of absorbance of plane-polarized light parallel to the direction of stretch ($A_\parallel$) will differ from the absorbance of plane-polarized light perpendicular to the direction of stretch ($A_\perp$). The ratio of these two absorbances is called the dichroic ratio D,

$$D = A_\parallel / A_\perp \tag{1}$$

which varies from zero to infinity, with unity representing random orientation. The orientation of transition moment vector f_M can be related to the stretch direction by the following expression[26]:

$$f_M = \frac{D - 1}{D + 2} \tag{2}$$

To relate the orientation of the polymer chain to the stretch direction, one must assume that all orientations of M about the chain axis are equally probable. The resulting transformation gives

$$f = \left(\frac{D_0 + 2}{D_0 - 1}\right)\left(\frac{D - 1}{D + 2}\right) \tag{3}$$

where D_0 is the dichroic ratio for perfect orientation and is related to the angle α between the transition moment vector M and the chain axis by the following equation:

$$D_0 = 2 \cot^2 \alpha \tag{4}$$

Thus, with the knowledge of the angle α and measurement of $A_\parallel$ and $A_\perp$, one can calculate the orientation function of the polymer chains.[27,28] Additionally, by studying absorptions of functional groups on different segments in block copolymers or on different components in blend systems, one can study the orientation of specific chain segments in complex multiphase polymer systems.

RESULTS AND DISCUSSION

Thermal Analysis

In Figure 1, the first heating thermogram of series 1 samples is shown as a solid line. Superimposed on each thermogram is the subsequent heating curve (dashed line) for the same sample after it had been cooled down from the molten state, at a rate of 20°C/min. The T_g data are summarized in Table I. A comparison of the two curves illustrates that in the first run, the glass transition region of PTMO is usually broader and the T_g determined is higher than that of the second run. In the first run, the PVC T_g is either not discernible or at a lower temperature than in the second run. In the second run, there are two distinct T_g's, each of which corresponds to that of the blend components. This suggests that THF solution casting produces phase mixing between PTMO and PVC in the series 1 samples. However, after heating into the melt and cooling, the same polyblend becomes incompatible.

It is noteworthy that, after a longer aging period at room temperature, the phase separation becomes more complete causing lower (PTMO) and higher (PVC) T_g's. This time-dependent phase mixing and demixing behavior which

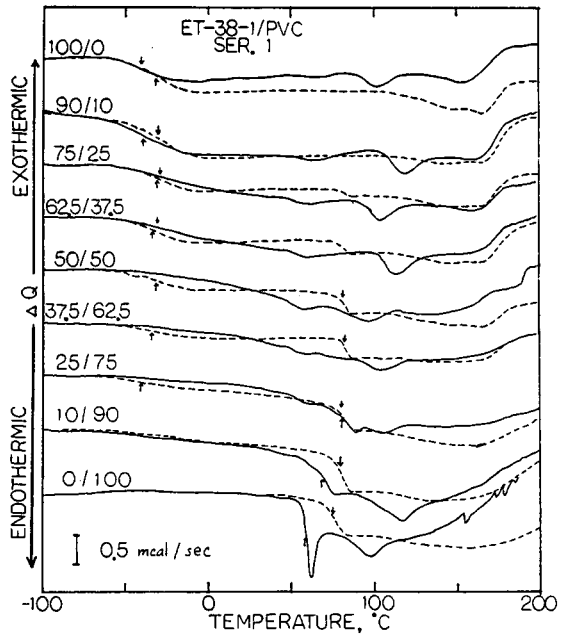

Fig. 1. DSC curves for series 1 blends (the first and the second heating thermograms).

has been discussed by Wilkes et al.[29] explains the seemingly contradictory results for 90/10 and 100/0. Finally, the slightly lower T_g (PVC) in high PVC content blends (e.g., 25/75, 10/90, and 0/100) may be due to trace amounts of solvent (THF) in the samples.[30]

In Figure 2, a heating curve is shown for each sample which has been quenched from the melt at a rate of 320°C/min. The T_g of PTMO is raised by 20 to 30°C, indicating phase mixing between the soft (PTMO) and the hard (MDI-BD) segments of ET-38-1. A distinct glass transition of PVC shows the inherent incompatibility between PTMO and PVC phases in samples quenched from the melt.

The DSC traces of series 2 samples are shown in Figure 3. This system is incompatible as illustrated by the two separate glass transitions originating from each blend component. Similar behavior is also observed in the compression molded (series 3) samples. In series 2 and 3 samples, the second DSC heating curve for the samples (not shown) was nearly identical to the first trace.

Figures 1 to 3 illustrate that by applying different sample preparation methods, one obtains a partially compatible system in series 1 and an incompatible polyblend in both series 2 and 3. Although PTMO (soft segment phase of ET-38-1) and PVC are incompatible, because both ET-38-1 and PVC are soluble in THF, a compatible ET-38-1/THF/PVC system in solution is formed. At the beginning of spin casting, THF preserves the phase mixing; and after most of the solvent has been removed, the system becomes too viscous to form separate phases at room temperature. Therefore, a kinetically controlled or metastable mixed state is obtained. For series 2 samples which were prepared using a solvent mixture of THF/*p*-dioxane, after the removal of most of THF (bp = 66°C), PVC precipitates, as it is insoluble in the remaining *p*-dioxane (bp = 101°C). Thus, in

TABLE I
Glass Transition Temperatures of ET-38-1/PVC Blends (DSC Data), °C

ET-38-1/PVC	FIRST	SECOND	QUENCH
SERIES ONE			
100/0	-41	-32, -	-10, -
90/10	-39	-30, -	-9, -
75/25	-29	-31, 81	-12, 83
62.5/37.5	-31	-34, 81	-11, 83
50/50	-	-31, 81	-11, 82
37.5/62.5	-	-34, 82	-16, 83
25/75	80	-41, 79	-19, 83
10/90	68	- , 79	- , 81
0/100	59	- , 75	- , 78
SERIES TWO			
100/0	-41, -		
75/25	-40, 92		
62.5/37.5	-35, 91		
50/50	-34, 92		
37.5/62.5	-32, 89		
25/75	-41, 90		
0/100	- , 87		
SERIES THREE			
75/25	-39, 83		
62.5/37.5	-42, 82		
50/50	-41, 80		
37.5/62.5	-48, 82		
25/75	-47, 80		

the presence of some *p*-dioxane, ET-38-1 forms a continuous matrix from which PVC precipitates. Upon melt processing, ET-38-1 and PVC also formed separate phases as evidenced by the results of series 3.

Dynamic Mechanical Properties

The storage modulus (E') and the dissipation factor (tan δ) of series 1 and 2 samples are plotted as a function of temperature in Figures 4 and 5. Peak positions in the tan δ curves from these figures are summarized in Table II. Despite the difference in sample preparation methods, two maxima in the tan δ curve for pure ET-38-1 occur at approximately −125 and −5°C. The low-temperature loss peak is due to the local motion of the —$(CH_2)_4$—O— group.[31,32] The high-temperature loss peak is attributed to the motion of the soft segment PTMO which accompanies the glass transition. The storage modulus E' decreases very gradually after the glass transition, indicating that microphase separation of the hard segments takes place and provides a self-reinforcement of the elastomer leading to unusually high modulus values.[33,34] Pure PVC also shows two maxima

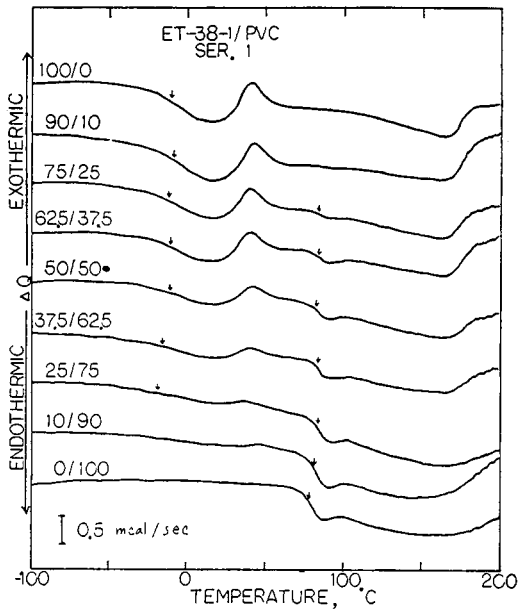

Fig. 2. DSC curves for series 1 blends (quenched samples).

located at −25 and 90°C, respectively. The broad low temperature loss peak is ascribed to local mode motion of the main chain, while the high-temperature damping is related to relaxation associated with the glass transition.[35]

In series 1 blends, the appearance of a single glass transition suggests phase

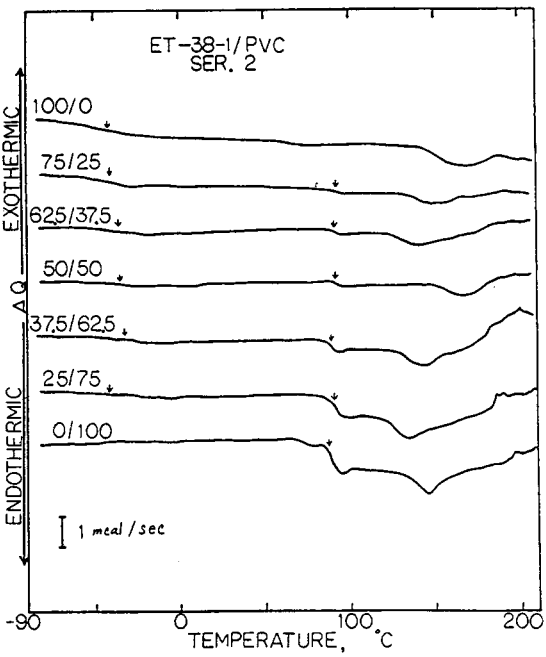

Fig. 3. DSC curves for series 2 blends.

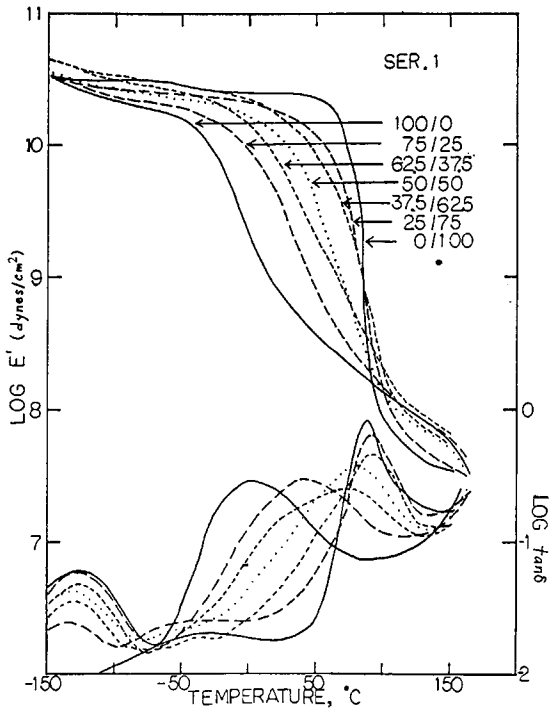

Fig. 4. Storage modulus E' and tan δ curves of series 1 blends.

mixing of the segments of PVC and ET-38-1. The increase in T_g is due to an increase in the PVC content of the amorphous polyether phase of the polyurethane. However, in all of the blends, the α-transition is broader than it is for either pure component alone which suggests a certain degree of heterogeneity for these partially compatible blends. The observed change in the local mode dispersion (−25°C peak) of PVC indicates that the local environment of PVC segments has been altered by the presence of polyether segments. As the polyurethane content is increased, the weak shoulder shifts to a lower temperature, showing behavior similar to that which occurs in plasticized PVC systems.[36]

The data for both series 2 and 3 blends show two transitions at approximately −10°C (α_1) and 100°C (α_2) which are due to the backbone motion of polyether portion of the polyurethane and PVC, respectively. Since each phase is pure enough to exhibit its own glass transition, series 2 and 3 samples are considered to be incompatible, and therefore the observed different magnitudes of either tan δ peak height or E' plateau level for different samples are only a function of the relative amount of each component.

While PTMO and PVC are partially compatible in series 1 and incompatible in series 2 and 3, MDI-BD forms a distinct phase in all three series of blends and acts as a filler of high modulus. It is also noted that at room temperature the storage modulus E' of series 1 blends is greater than that of the corresponding samples (same composition) is series 2 and 3. This is consistent with the stress–strain measurements and is discussed in the following section.

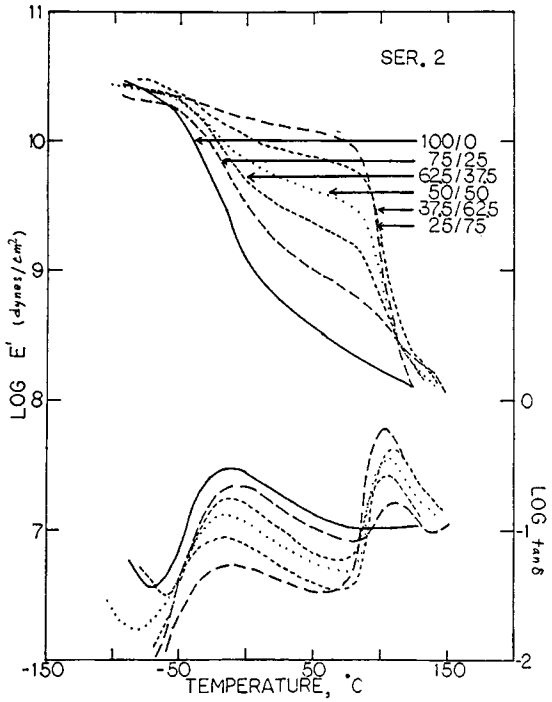

Fig. 5. Storage modulus E' and tan δ curves of series 2 blends.

Tensile Properties

Only the stress–strain curves for series 1 blends are shown here (Fig. 6) since both series 2 and 3 samples show very similar responses. All stress-strain data are summarized in Table III. These data are an average from three runs for ultimate strength, Young's modulus, and elongation at failure. Stresses have been calculated on the basis of the initial cross-sectional area. It should also be noted that the percent elongation is the true strain determined using an extensometer accessory.

For all three series of blends, an increase in the ET-38-1 content generally reduced the Young's modulus and greatly increased the elongation at failure. PTMO appears to act as an effective "plasticizer" for PVC in all the blends. Although blends of series 2 and 3 are incompatible, based on the results from DSC and Rheovibron, there must exist substantial interaction of the two blending components (such as effective interfacial bonding) since rather good mechanical properties are obtained. Thus, the blends of series 2 and 3 can be called mechanically compatible,[37] since their mechanical properties are enhanced over those which would be obtained from a truly incompatible system. Similar behavior has been shown for blends of polycaprolactone with poly(vinyl acetate), polystyrene, or poly(methyl methacrylate).[37]

Because the stress–strain testing was done at room temperature, the results depend strongly upon the viscoelastic state of the specimens. The dynamic mechanical data indicate that, at room temperature, series 1 samples are near T_g in the leathery region, while series 2 and 3 are both in the rubbery state if only the continuous PTMO phase is considered. Because PVC has a higher T_g than

TABLE II
Glass Transition and Secondary Relaxation of ET-38-1/PVC Blends (Rheovibron Data), °C

ET-38-1/PVC	GLASS TRANSITION	SECONDARY RELAXATION
SERIES ONE		
100/0	5	-126, -
75/25	40	-126, -
62.5/37.5	75	-127, -
50/50	80	-130, -40
37.5/62.5	91	-130, -35
25/75	92	-135, -30
0/100	91	- , -25
SERIES TWO		
100/0	-8, -	
75/25	-5, 112	
62.5/37.5	-10, 106	
50/50	-16, 105	
37.5/62.5	-15, 110	
25/75	-10, 104	
SERIES THREE		
100/0	-8, -	-125, -
75/25	-8, 100	-123, -
62.5/37.5	-15, 98	-122, -
50/50	-20, 100	-123, -
37.5/62.5	-22, 100	-122, -
25/75	-20, 100	-123, -
0/100	- , 92	- , -25

PTMO, the partially compatible blends (series 1) are stiffer than the incompatible samples (series 2 and 3). This is verified by comparing the Young's moduli for blends of the same compositions.

Infrared Spectrum Peak Positions

If there are acid–base or other attractions between chemical groups on the dissimilar polymer segments, the peak positions of the participating groups should shift to reflect this interaction. This is the behavior for a compatible blend which shows an extensive phase mixing. However, the peak positions do not shift in an incompatible system because segmental environment is not affected by blending. In both the IR peak position and IR dichroism studies, only series 1 and 2 blends were studied since the required thin films for IR could not be prepared by compression molding.

The hard segment (MDI-BD) of ET-38-1 contains both N—H and C=O groups. Most of these MDI-BD segments reside in hard segment domains; however, due to an incomplete phase separation some hard segments are dispersed in the PTMO–PVC (series 1) or PTMO (series 2) matrix.

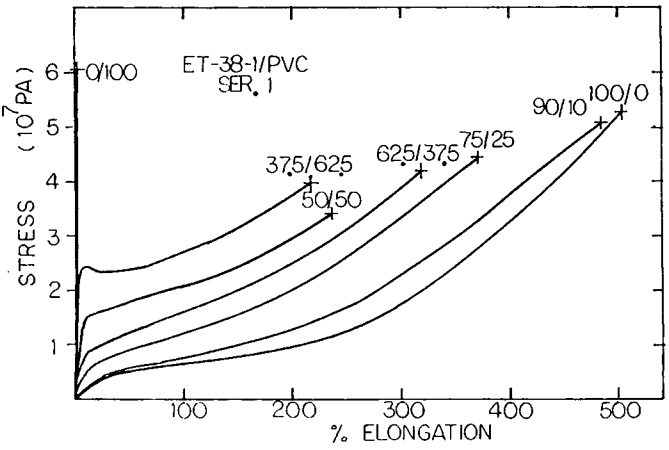

Fig. 6. Stress–strain curves for series 1 blends.

The N—H protons and the C=O oxygens which form hydrogen bonds are designated as hydrogen-bonded N—H (NH_B) and hydrogen-bonded C=O (CO_B). On the other hand, for the isolated MDI-BD segment which is phase-mixed with the soft-segment matrix, most of the C=O groups are free (CO_F) or nonhydrogen bonded. It was of interest to observe the peak positions of NH_B, CO_B, and CO_F as a function of blend composition in order to discover if specific interaction could be found between ET-38-1 and PVC in both the compatible (series 1) and incompatible (series 2) systems.

In both series of blends, the NH_B peaks as a function of blend composition stay within a range of 1 cm^{-1} (Fig. 7). Similar behavior is exhibited by the CO_B peaks. This indicates urethane hard-segment phase separation in blends of series 1 and 2. However, the CO_F in series 1 samples shows a significant shifting to lower frequency with increasing PVC concentration compared to the blends of series 2 whose CO_F remains unchanged (Fig. 7). The series 1 free carbonyls appear to be influenced by the α-hydrogen (H_α) on the PVC in the compatible PTMO–PVC system.

The PVC infrared spectrum has been very well characterized.[38,39] The C—Cl stretching peak at about 611 cm^{-1} represents extended chain segments of syndiotactic sequences (CCl_S) while the 637 cm^{-1} C—Cl stretching band is a collection of isotactic and syndiotactic ($CCl_{I,S}$) sequences. The 611 and 637 cm^{-1} peaks do not shift upon blending of PVC with ET-38-1.

The C—H_α peak in the IR spectra of the series 1 blends may be expected to shift in a similar fashion to the CO_F peak. Unfortunately, the IR spectra of ET-38-1 and PVC overlap in this C—H stretching region making C—H peak position studies very difficult.

Infrared Dichroism

The NH_B and CO_B groups were used to follow the orientation of the urethane hard segment while the orientation of the soft segment was followed by using the CO_F groups. This assumes that isolated MDI segments in the soft segment domains will orient in a similar fashion to the polyether segments. Both of the

TABLE III
Tensile Properties of ET-38-1/PVC Blends

ET-38-1/PVC	ELONGATION AT FAILURE %	ULTIMATE TENSILE STRENGTH (10^7 Newton/m^2)	YOUNG'S MODULUS (10^7 Newton/m^2)
SERIES ONE			
100/0	505	5.26	3.54
90/10	484	5.09	4.55
75/25	370	4.44	12.57
62.5/37.5	318	4.20	28.54
50/50	237	3.41	68.36
37.5/62.5	218	3.98	134.48
25/75	-	3.7*	207
10/90	-	4.2*	301
0/100	2	5.95	371
SERIES TWO			
100/0	614	3.37	4.82
75/25	385	2.8	13.20
62.5/37.5	310	2.74	20.05
50/50	378	4.15	38.27
37.5/62.5	316	4.09	89.08
25/75	-	3.2*	74.71
0/100	-	-	262
SERIES THREE			
100/0	579	4.8	4.91
75/25	411	3.26	14.64
62.5/37.5	316	3.36	27.58
50/50	198	2.52	68.19
37.5/62.5	189	3.10	114
25/75	155	3.77	168
10/90	-	3.5*	270
0/100	-	4.7*	336

[a] Estimated Value.

C—Cl stretching peaks at 637 and 691 cm^{-1} are assumed to originate from amorphous-phase PVC chain segments. Orientation of the PVC phase was followed using the 637 cm^{-1} peak because it is both stronger and sharper than the 691 cm^{-1} peak. The transition moment vectors of the NH_B, CO_B, CO_F, and CCl were assumed to be respectively at 90, 78, 78, and 90° to the corresponding chain axis. The experimental data are only available up to 62.5% PVC because the films of higher PVC content are too brittle to be uniformly stretched.

Orientation functions for the NH_B and CO_B of each sample are very similar. This is due to the fact that both groups reside in the same hard-segment domain.

The CO_F orientation is observed greater than those of the NH_B and CO_B at low strain while the inverse is true at high elongations (Figs. 8 and 9). This suggests that microphase separation in the polyurethane occurs in both blend systems. Initially, the stiffer hard segment domains are less affected by

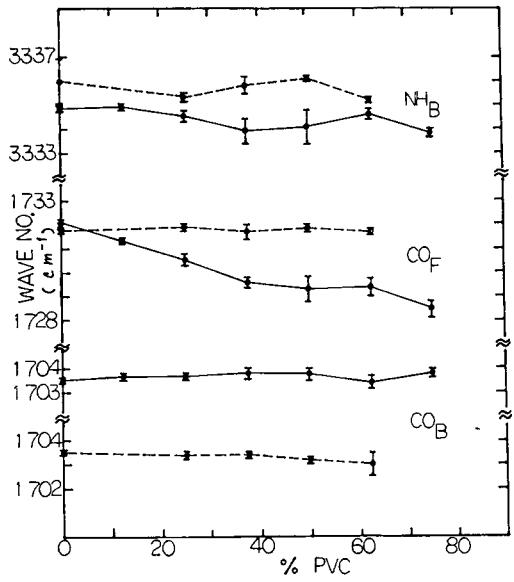

Fig. 7. Infrared peak positions of series 1 and 2 blends (NH_B, CO_B, and CO_F). (—) Series 1; (- - -) Series 2.

stretching, while the coiled soft segments are easily oriented because they are above their T_g. As the film is elongated, the soft segments apply increasing shear stress to the hard segments, causing them to orient into the stretch direction. It should be noted that the dichroism data were taken after 10 min of stress relaxation. Consequently, the soft segments tended to disorient toward a more random conformation via an entropy-driven mechanism. The accompanying retractive force exerts a tension on the hard segments, causing them to become further aligned in the stretch direction.

Because ET-38-1 absorbs strongly in the 700 to 600 cm^{-1} range, the PVC di-

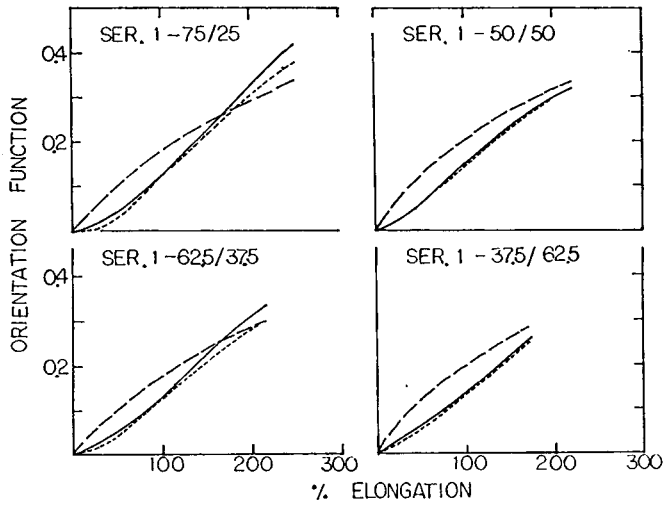

Fig. 8. Orientation function vs. elongation curves of series 1 blends (f_{CO_B}, f_{CO_F}). (—) NH_B; (- - -) CO_B; (— — —) CO_F.

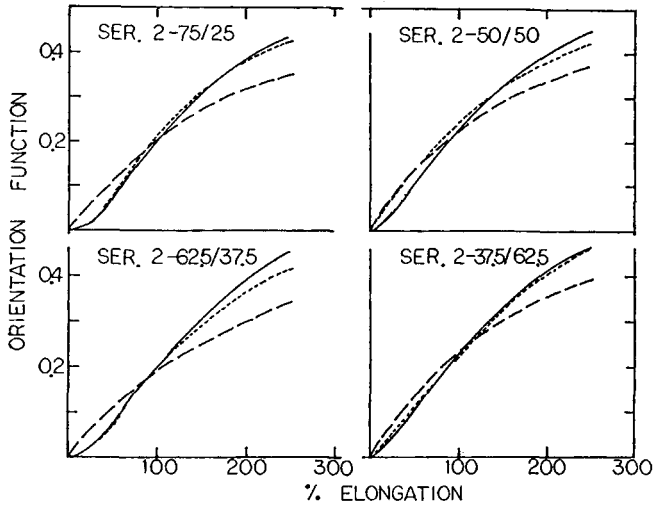

Fig. 9. Orientation function vs. elongation curves of series 2 blends (f_{CO_B}, f_{CO_F}). (—) NH_B, (- - -) CO_B, (— — —) CO_F.

chroism studies were only done for 62.5/37.5, 50/50, and 37.5/62.5 samples. For series 1 samples, at low strain, the CCl orientation is similar to that of the CO_F (Fig. 10). However, the orientation functions of CCl and CO_F are well separated for the corresponding samples in series 2. The similarity suggests that the local environment is very much the same for both PTMO and PVC in the series 1 compatible blends.[21]

For the 37.5/62.5 blends, the match of CCl and CO_F orientation for series 1 sample at low strains indicates the segmental compatibility between PTMO and PVC phases (Fig. 11). However, at higher strains, the CCl orientation is observed to be higher than those of CO_F in both series of blends. It appears that, for the series 1 sample, the PTMO–PVC compatible matrix is PVC-rich and shows

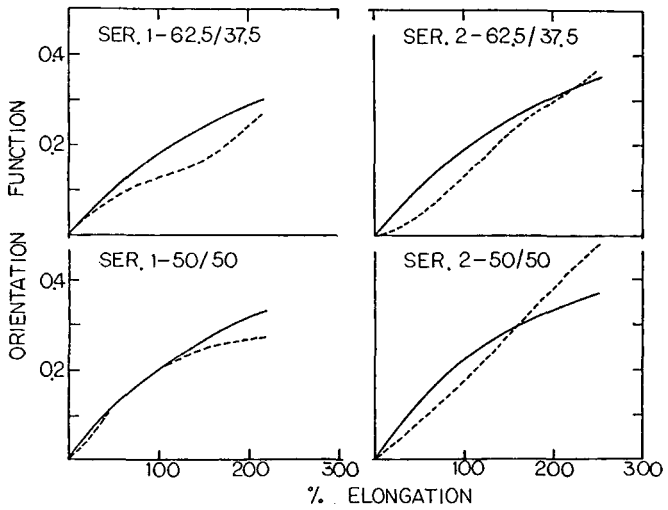

Fig. 10. Orientation function vs. elongation curves of series 1 and 2 blends (f_{CO_F}, f_{CCl} for 62.5/37.5 and 50/50 compositions). (—) CO_F, (- - -) CCl.

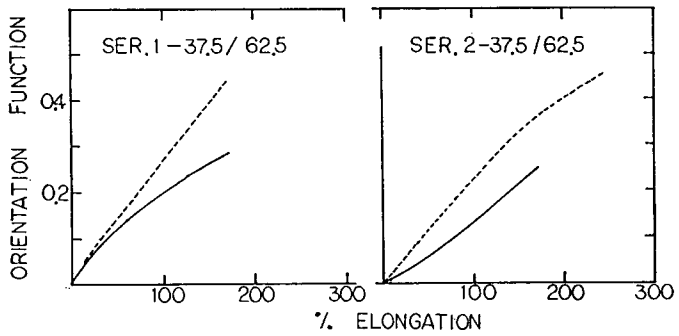

Fig. 11. Orientation function vs. elongation curves of series 1 and 2 blends (f_{CO_F}, f_{CCl} for 37.5/62.5 composition). (—) CO_F, (- - -) CCl.

similar orientation of CCl and CO_F only at low strains. In the series 2 samples, the PVC and polyurethane chains reside in two interconnecting matrices, with the more rigid PVC segments showing higher orientation at all strain levels.

Morphological Models

A morphological model of series 1 blends is shown in Figure 12 and is similar to Estes' model for polyurethane block polymers.[40] The heavy lines represent hard segments which aggregate into hard domains. Shorter hard segments may be dispersed in the matrix phase which is a compatible PTMO–PVC mixture.

Figure 13 shows a model for series 2 and 3 blends of ET-38-1/PVC. The

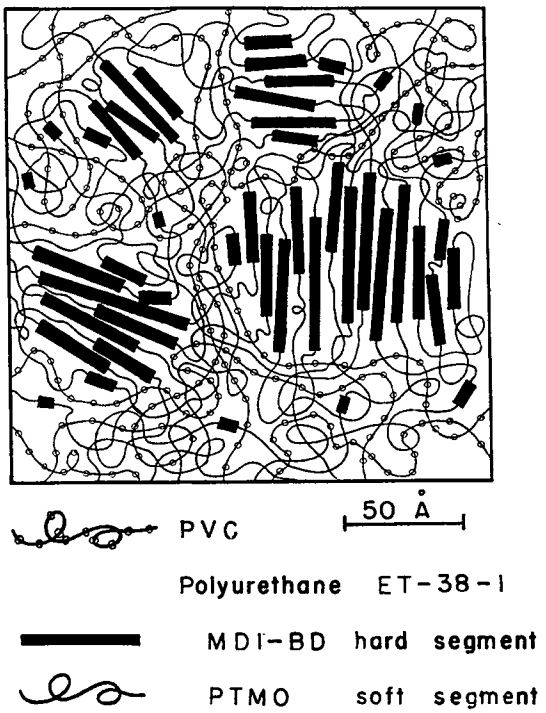

Fig. 12. Morphological model of the series 1 blends (for 50/50 composition).

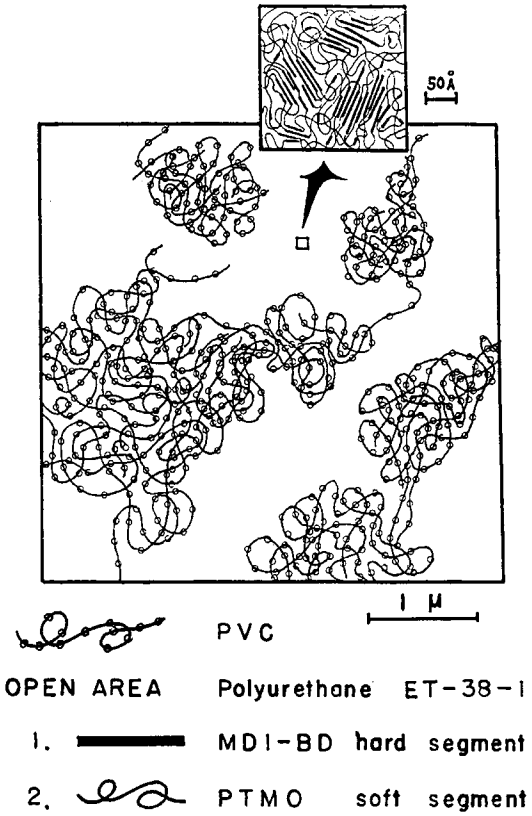

Fig. 13. Morphological model of the series 2 and 3 blends (for 50/50 composition).

MDI-BD domains still have the same morphology as in the series 1 samples but are not visible at the scale of this representation. The PVC domains exist either as an inclusion or as an interconnecting network depending on PVC concentration.

Microscopic Studies

Bright-field transmission studies were made on a Jelco 100B microscope with an accelerating voltage of 60 kv. Preliminary observations on series 2 specimens, prepared by ultramicrotoming, show PVC domains as slightly darker regions because of their greater electron density. The width of these domains is on the order of a micron, though in most cases the image contrast was not high enough to clearly show the morphology of the polyurethane and PVC phases. Further work utilizing dehydrohalogenation treatment of the PVC component to introduce unsaturation[41] amenable to staining with OsO_4 is underway.

CONCLUSIONS

DSC, Rheovibron, stress–strain, IR peak position studies, and IR dichroism experiments were used to characterize the thermal, dynamic mechanical, mechanical, and morphological properties of the ET-38-1/PVC blends prepared

by different methods. As determined from DSC and Rheovibron data, series 2 and 3 samples are incompatible while series 1 is partially compatible. However, similar uniaxial stress–strain data on all three series of blends indicate substantial polyether (ET-38-1 soft segment) plasticization effect upon PVC, and therefore all of the blends can be considered as mechanically compatible. IR peak shifts and IR dichroism results both suggest segmental compatibility in series 1 samples and an intrinsic incompatibility for series 2 and 3 samples.

The authors wish to acknowledge partial support of their work by NSF's polymer program of the Division of Materials Research through Grant DMR-78-11662 and the Naval Air Systems Command through Contract # N00019-80-C-0367.

References

1. D. A. Thomas, *J. Polym. Sci. Polym. Symp.*, **60,** 189 (1977).
2. V. Huelck, D. A. Thomas, and L. H. Sperling, *Macromolecules*, **5,** 340 (1972).
3. S. L. Aggarwal, *Polymer*, **17,** 938 (1976).
4. S. D. Hong and M. Shen, *Polym. Sci. Technol.*, **10,** 77 (1977).
5. T. Nishi, T. K. Kwei, and T. T. Wang, *J. Appl. Phys.*, **46,** 4157 (1975).
6. L. E. Nielsen, *Mechanical Properties of Polymers and Composites*, Marcel Dekker, New York, 1974.
7. T. Nishi and T. K. Kwei, *J. Appl. Polym. Sci.*, **20,** 1331 (1976).
8. W. J. MacKnight, J. Stoelting, and F. E. Karasz, *Adv. Chem. Ser.*, **99,** 29 (1971).
9. J. A. Sauer and A. E. Woodward, *Rev. Mod. Phys.*, **32,** 88 (1960).
10. M. M. Coleman, J. Zarian, D. F. Varnell, and P. C. Painter, *J. Polym. Sci. Polym. Lett. Ed.*, **15,** 745 (1977).
11. L. W. Kleiner, F. E. Karasz, and W. J. MacKnight, *Soc. Plast. Eng. Annual Tech. Conf.*, 243 (1978).
12. J. Stoelting, F. E. Karasz, and W. J. MacKnight, *Polym. Eng. Sci.*, **10**(3), 133 (1970).
13. S. D. Hong, M. Shen, T. Russell, and R. S. Stein, *Polym. Sci. Technol.*, **10,** 77 (1977).
14. G. Akovali, M. Niinomi, J. Diamant, and M. Shen, *Polym. Prep. Am. Chem. Soc. Div. Polym. Chem.*, **17,** 560 (1976).
15. W. Rovatti and E. G. Bobalek, *J. Appl. Polym. Sci.*, **7,** 2269 (1963).
16. Y. J. Shur and B. Ranby, *J. Appl. Polym. Sci.*, **19,** 2143 (1975).
17. D. J. Hourston and I. D. Hughes, *J. Polym. Sci. Polym. Phys. Ed.*, **15,** 3099 (1977).
18. L. Bohn, *Rubber Chem. Tech. Rep.*, **41,** 495 (1968).
19. S. Krause, *J. Macromol. Sci. Rev. Macromol. Chem.*, **7,** 251 (1972).
20. G. A. Zakrzewski, *Polymer*, **14,** 348 (1973).
21. D. S. Hubbell and S. L. Cooper, *J. Polym. Sci. Polym. Phys. Ed.*, **15,** 1143 (1977).
22. F. B. Khambatta, F. Warner, T. Russell, and R. S. Stein, *J. Polym. Sci. Polym. Phys. Ed.*, **14,** 1391 (1976).
23. J. C. West and S. L. Cooper, *J. Polym. Sci., Polym. Symp.*, **60,** 127 (1977).
24. R. W. Seymour and S. L. Cooper, *Macromolecules*, **6,** 48 (1973).
25. L. J. Koberstein, S. L. Cooper, and M. Shen, *Rev. Sci. Instrum.*, **46,** 1639 (1975).
26. S. Nomura, H. Kawai, I. Kimura, and M. Dagiyama, *J. Polym. Sci., Part A-2*, **5,** 479 (1967).
27. R. S. Stein and F. H. Norris, *J. Polym. Sci.*, **21,** 381 (1956).
28. B. E. Read and R. S. Stein, *Macromolecules*, **1,** 116 (1968).
29. G. L. Wilkes and J. A. Emerson, *J. Appl. Phys.*, **47**(10), 4261 (1976).
30. J. Malac, V. Altmann, and J. Zelinger, *J. Appl. Polym. Sci.*, **14,** 161 (1973).
31. T. Nishi and T. K. Kwei, *J. Appl. Polym. Sci.*, **20,** 1331 (1976).
32. H. E. Bair, M. Matsuo, W. A. Salmon, and T. K. Kwei, *Macromolecules*, **5,** 114 (1972).
33. D. S. Huh and S. L. Cooper, *Polym. Eng. Sci.*, **11**(5), 369 (1971).
34. J. W. C. Van Bogart, A. Lilaonitkul, and S. L. Cooper, *Adv. Chem. Ser.*, **176,** 3 (1979).
35. M. Takayanagi, *Mem. Fac. Eng. Kyushu Univ.*, **23**(1), 11 (1963).
36. G. Pezzin, G. Ajroldi, and C. Garbrglio, *J. Appl. Polym. Sci.*, **11,** 2553 (1967).
37. G. L. Brode and J. V. Koleske, *J. Macromol. Sci., Chem.*, **A6,** 1109 (1972).

38. S. Krimm, V. L. Folt, J. J. Shipman, and A. R. Berens, *J. Polym. Sci., Part A*, **1**, 2621 (1963).
39. S. Krimm, V. L. Folt, J. J. Shipman, and A. R. Berens, *J. Polym. Sci., Part A*, **2**, 1009 (1964).
40. G. M. Estes, R. W. Seymour, and S. L. Cooper, *Macromolecules*, **4**, 452 (1971).
41. Y. Shindo, B. E. Read, and R. S. Stein, *Makromol. Chem.*, **118**, 272 (1968).

Received June 4, 1980
Accepted February 24, 1981